THE EVOLUTION OF FRICTION STIR WELDING THEORY AT MARSHALL SPACE FLIGHT CENTER

Ninth International Friction Stir Welding Symposium
Huntsville, AL, May 15-17, 2012

Arthur C. Nunes, Jr.
Materials and Processes laboratory,
Marshall Space Flight center, Huntsville, AL

ABSTRACT

From 1995 to the present the friction stir welding (FSW) process has been under study at Marshall Space Flight Center (MSFC). This is an account of the progressive emergence of a set of conceptual tools beginning with the discovery of the shear surface, wiping metal transfer, and the invention of a kinematic model and making possible a treatment of both metallurgical structure formation and process dynamics in friction stir welding from a unified point of view.

It is generally observed that the bulk of the deformation of weld metal around the FSW pin takes place in a very narrow, almost discontinuous zone with high deformation rates characteristic of metal cutting. By 1999 it was realized that this zone could be treated as a shear surface like that in simple metal cutting models. At the shear surface the seam is drawn out and compressed and pressure and flow conditions determine whether or not a sound weld is produced.

The discovery of the shear surface was followed by the synthesis of a simple 3-flow kinematic model of the FSW process. Relative to the tool the flow components are: (1) an approaching translational flow at weld speed V, (2) a rotating cylindrical plug flow with the angular velocity of the tool ω, and (3) a relatively slow ring vortex flow (like a smoke ring) encircling the tool and driven by shoulder scrolls and pin threads. The rotating plug flow picks up an element of weld metal, rotates it around with the tool, and deposits it behind the tool (“wiping metal transfer”); it forms plan section loops in tracers cut through by the tool. Radially inward flow from the ring vortex component retains metal longer in the rotating plug and outward flow expels metal earlier; this interaction forms the looping weld seam trace and the “tongue and groove” bimetallic weld contour. The radial components of the translational and ring vortex flows introduce parent metal intrusions into the small grained nugget material close to the tool shoulder; if this feature is pronounced, “nugget collapse” may result.

Certain weld features, in particular internal banding seen in transverse section as “onion rings” and associated surface ridges called “tool marks”, have long implied an oscillation flow component, but have only recently been attributed in the literature to tool eccentricity.

Rotating plug shape, typically a hollow cylinder flared at the end where it sticks to the shoulder, varies as pressure distribution on the tool determines where sticking occurs. Simplified power input estimates balanced against heat loss estimates give reasonable temperature estimates, explain why the power requirement changes hardly at all over a wide range of RPM’s, and yield isotherms that seem to fall along boundaries of parameter windows of operation.

Key, apparently complex structural and dynamic features of the FSW welding process seem to have been successfully modeled and understood.

1995: FSW COMES TO MSFC

In 1995 Marshall Space Flight Center (MSFC) engineer Jeff Ding brought a friction stir welding (FSW) apparatus to MSFC to see if solid state welding could eliminate fusion-welding problems of the new Li-containing aluminum alloy mandated for the Light Weight Space Shuttle External Tank.

The author of this paper was assigned to study the physical basis of the FSW process. While technology per se does not require that its developers understand it, and much technological development has been and still is carried out by pure cut-and-try experimentation, understanding the physical basis of what one is doing suggests innovations, reduces risk of dangerous mistakes or wasted effort, and is occasionally critical to solving problems [1] holding back development. The MSFC welding group has long backed up its technological development efforts with research into the fundamentals underlying the technology.

At the time the earliest notions of FSW as chaotic mixing had given way to the "extrusion theory" of the friction stir mechanism. Frictional heating at the tool/metal interface was conceived as softening the weld metal adjacent to the tool. The softened metal was extruded back around the tool as the tool moved forward.

It was not clear what friction coefficient should be used. Nor was it clear how the extrusion theory related to tracer experiment results [2,3] or to the complex structural features of the weld. There was a mental image of a mechanism, but no real understanding, neither kinematic nor dynamic, of the process.

LATE 90's: THE DISCOVERY OF THE SHEAR SURFACE

Records no longer preserve the precise year, perhaps it was 1998, in which it was realized that the sharp cylindrical interface seen in Figure 1 between parent metal and the finely recrystallized metal in the wake of the FS weld could be treated as a shear surface like the shear surface in the shear plane model of the metal cutting process [4]. In metal cutting, chips with the same kind of extreme grain refinement as in the FS weld wake are observed [5].

An estimate of the mean shearing rate $\dot{\gamma}$ across the shear surface can be made.

$$\dot{\gamma} \sim \frac{r\omega}{\delta} \qquad (1)$$

In equation (1) r is the radius of the shear surface, ω is the angular velocity of the metal inside the shear surface (taken to be approximately the same as that of the tool), and δ is the thickness across the shear surface. Scaling δ very roughly from Figure 1 at 0.001 inch implies a shear rate of 4×10^3 sec^{-1}.

In the following years it became clear how the shear surface, essentially an "adiabatic shear zone" [6,7], depends upon a strain-rate insensitive (plastic) constitutive equation. The shear surface is embedded in a widely distributed, slower flow field, possibly a viscous creep. The author has generally ignored the *rotational* "viscous creep" component, but the *radial* and *axial* components (embodied in the ring vortex flow

component--see below) have very visible effects upon weld structure and must be taken into account.

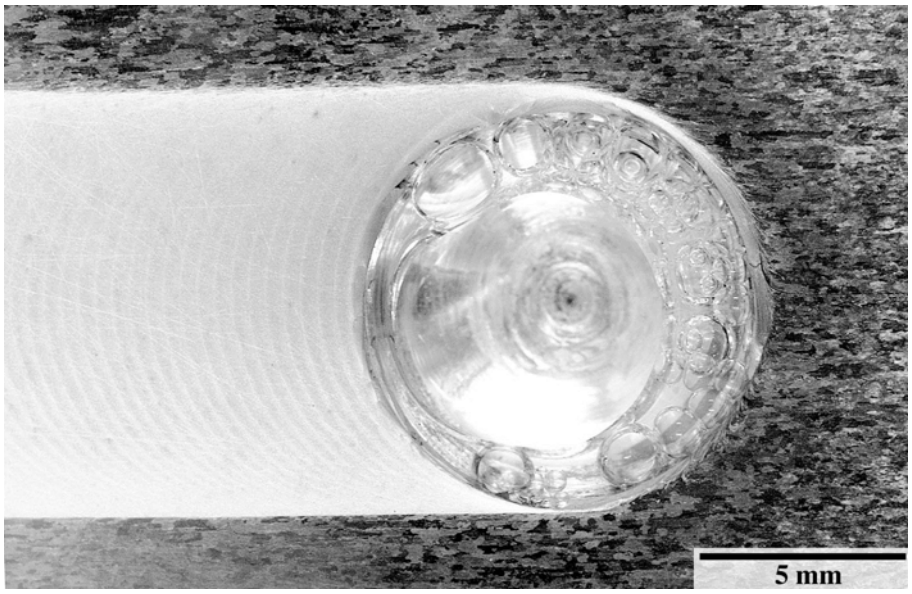

Figure 1. Midsectional plan-view of macrostructure around FSW pin, tool spindle rotating counterclockwise at 220 RPM, travel to the right at 3.5 inches per minute in 0.317 inches thick 2219-T87 aluminum alloy. The weld was suddenly stopped and the pin backed out of its cavity, which has been replaced by a bubble-filled mounting medium. Note the very sudden refinement in structure at the shear surface. Note the increased thickness of the rotating plug of weld metal beneath the shear surface on the retreating edge of the pin to accommodate backflow of metal around the pin. In sections closer to the shoulder the shear surface moves out to enclose a wider expanse of rotating plug metal.

1999: KINEMATIC FSW MODEL

In 1999 things came together and the simplified kinematic FSW model emerged [6,7,8,9]. The model was comprised a superposition of three components: 1. a uniform translation of $-V$ with respect to the tool, 2. a rotating cylindrical plug of radius r and angular velocity ω embedded in a continuum, and 3. a ring vortex circulation like a smoke-ring encircling the tool with local radial and axial velocity field components specified as needed. Each component flow field ($\vec{V}_1, \vec{V}_2, \vec{V}_3$) is simple enough so that it can be seen by inspection to conserve volume. Hence the superposition $\vec{V}_1 + \vec{V}_2 + \vec{V}_3$ also conserves volume:

$$\nabla\cdot\left(\vec{V}_1+\vec{V}_2+\vec{V}_3\right)=\nabla\cdot\vec{V}_1+\nabla\cdot\vec{V}_2+\nabla\cdot\vec{V}_3=0+0+0=0 \qquad (2)$$

ROTATING PLUG EFFECTS

The main effect of a rotating plug superposed upon a translating flow is to rotate, then release those elements of weld metal encountering the plug. Originally we took a merry-go-round as an analogue for the rotating plug as shown in Figure 2. If one were to walk straight across a rotating platform, the radial velocity component would initially take one deeper onto the rotating platform, then, with the shift onto the opposite side brought about by the platform rotation, the radial velocity component would take one back off the platform. Symmetry would take one off the platform along the same line as upon entering.

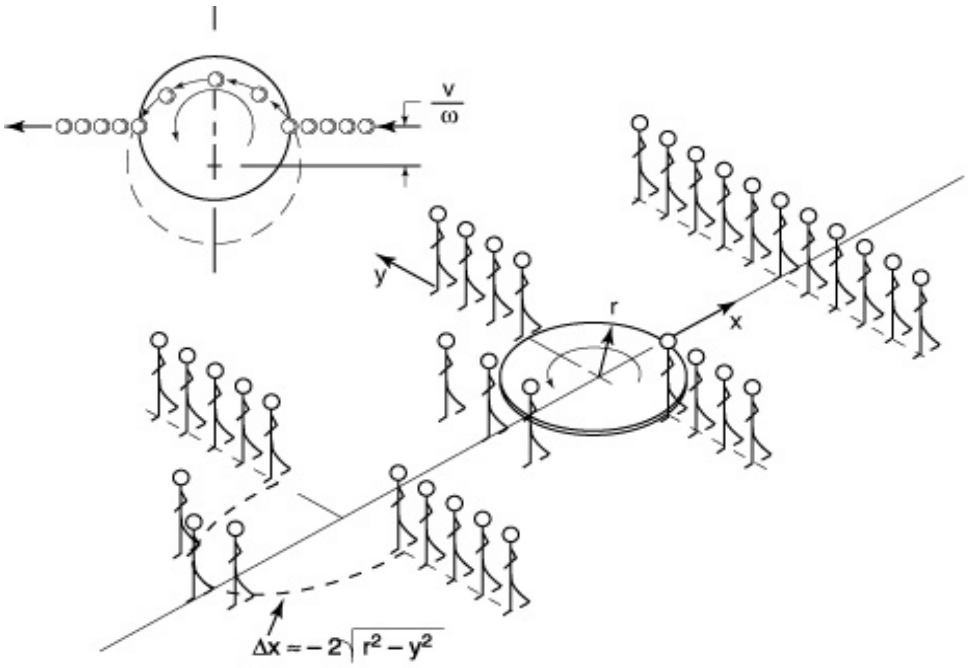

Figure 2. Early presentation (internal 14 February 2000) of the rotating plug model. A segment of the line of marching figures marches across a merry-go-round platform and is whisked forward. A similar displacement occurs when a rotating plug runs through a tracer line [2].

The radial trajectory of an element of metal inside the rotating plug is approximately:

$$r \sim r_o - \frac{V}{\omega}\left(\frac{y}{r} - \frac{y_o}{r_o}\right) \qquad (3)$$

where r is the radius of the element from the shear surface center, r_o is the radius at which the element enters the rotating plug, y is the lateral displacement of the metal element toward the retreating side of the tool y_o is the lateral displacement at which the element enters the rotating plug, V is the tool translation speed, and ω is the tool angular velocity.

The distance inside the shear surface of a given streamline is $r_o - r$. This distance is zero upon entrance (wiping on) and again zero at exit (wiping off). If the radius of the shear surface remains constant at r_o, the trajectory of a flow streamline moves into the rotating plug initially, then outward, and finally encounters the shear surface again at $y = y_o$ and exits with lateral displacement unchanged.

A.P. Reynolds et al [2] show the parabolic loop formed by this mechanism in a tracer oriented the pressure perpendicular to the direction of tool motion.

But suppose that the plug radius oscillates, such that

$$r_o \rightarrow r_o + \Delta r \sin(\theta - \theta_o) \qquad (4)$$

Then, the distance inside the shear surface is $r_o + \Delta r \sin(\theta - \theta_o) - r$, which, substituting r from equation (3), becomes zero (streamline exit) when:

$$\frac{y}{r} \sim \frac{y_o}{r_o} - \frac{\omega \Delta r}{V} \sin(\theta - \theta_o) \qquad (5)$$

Such periodic variations in lateral displacement of the weld seam in plan section are commonly observed as in Figure 3. Less distinctly regarding periodicity, the same periodic variations are exhibited in lateral displacements of Kevin Colligan's shot tracers [3], but only near the shoulder, where shifts in the edge of the sticking area on the shoulder cause maximal variation Δr in the shear surface radius.

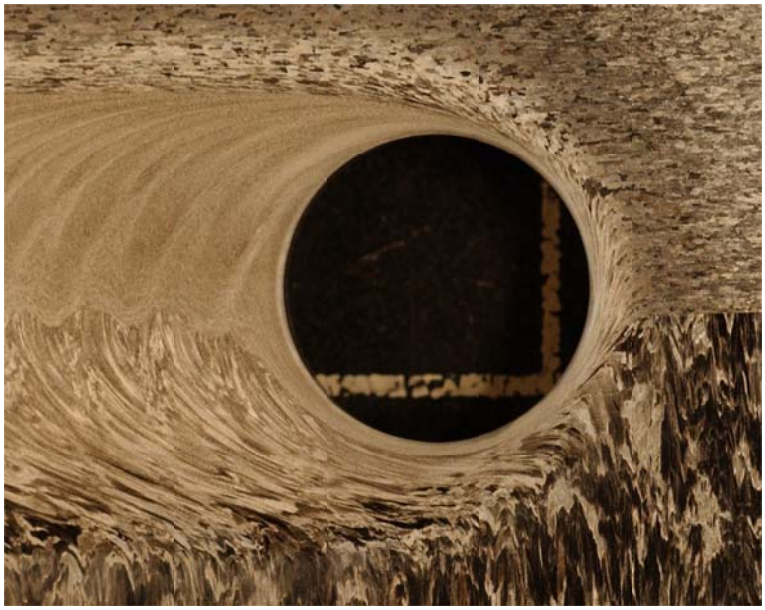

Figure 3. Lateral weld seam oscillation on plan-view of bimetallic FS weld: 2219 aluminum alloy on upper (advancing) side, 2195 on lower (retreating) side courtesy of G. Bjorkman of Lockheed Martin. Pin site (central hole) is 12.7 mm (0.5 inch) in diameter. The straight, unwelded seam on the right of the central hole becomes the wavy, welded seam on the left. While the 2219 metal appears to have entered the shear surface and been subjected to the grain refinement produced by its high shear rate, the 2195 metal appears to have been rotated around the tool in a slower peripheral flow resulting in a broader flow region and retaining more of the parent metal structural features.

Weld metal flows around the tool in an eccentric crescent of metal of thickness $\delta(\theta)$ incorporated into the rotating plug. The crescent is obvious in Figure 1, where the pin occupies almost all the area inside the crescent. Flow enters the forward shear surface at volume rate $(V\cos\theta)r d\theta$, and is removed at volume rate $r\omega d\delta$. By equating the two and integrating:

$$\delta = \frac{V}{\omega}(1+\sin\theta) \tag{6}$$

It will be noted that the eccentricity $\frac{2V}{\omega}$ needed to accommodate backflow around the tool by “wiping metal transfer” is not very large.

RING VORTEX EFFECTS

The ring vortex is characterized by a radial velocity v, taken positive outwards. It alters the trajectory of a streamline in the rotating plug (not the boundary of the plug or shear surface as discussed above).

$$r \sim r_o - \frac{V}{\omega}\left(\frac{y}{r} - \frac{y_o}{r_o}\right) + \frac{v}{\omega}(\theta - \theta_o) \tag{7}$$

This, too, causes a lateral shift. If the radius of the rotating plug remains constant at r_o, then

$$\frac{y}{r} \sim \frac{y_o}{r_o} + \frac{v}{V}(\theta - \theta_o) \tag{8}$$

If $\frac{y_o}{r_o} << 1$ and $\frac{v}{V} << 1$, then $\theta - \theta_o \sim \pi$ and $\frac{y}{r} \sim \frac{y_o}{r_o} + \pi\frac{v}{V}$, that is there is a lateral shift

$\Delta\left(\frac{y}{r}\right) \sim \pi\frac{v}{V}$.

Hence close to the shoulder, where the radial flow component v is inward/negative, the trace of the weld seam is displaced toward the advancing side of the tool, while at the root of a conventional weld or at the middle of a self-reacting weld, where radial flow component v is outward/positive, the trace of the weld seam is displaced toward the retreating side of the tool. The trace of the originally vertical seam is distorted into a loop starting on the advancing side of the weld and bellying out on the retreating side. This feature is particularly apparent in bimetallic welds where the metals exhibit etching contrast. Due to the seam loop, a "tongue and groove" structure is exhibited by bimetallic welds as shown schematically in Figure 4.

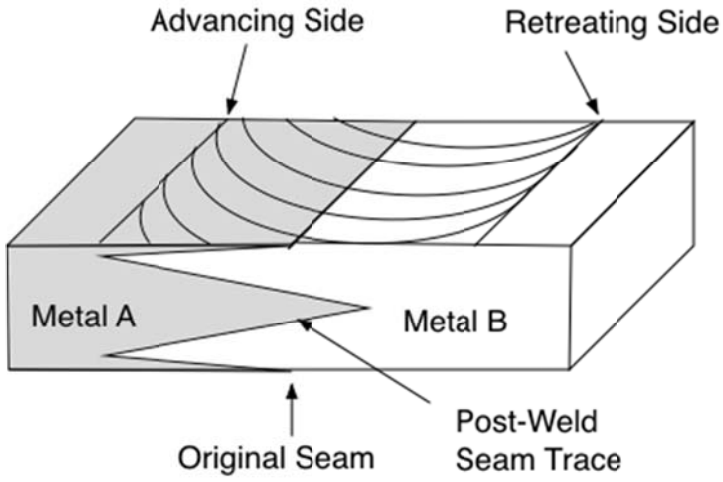

Figure 4. Schematic "tongue and groove" structure of bimetallic self-reacting weld. Where the ring vortex flow is radially inward the seam trace is held longer in the rotating plug and consequently is shifted toward the advancing side of the weld. At the weld center the ring vortex flow is radially outward, the seam trace is jettisoned sooner to the wake, and the seam trace is shifted to the retreating side of the weld. This sketch shows only general trends and not the usual complications that round off and distort the seam trace. Nor does it show other features that would be superimposed upon a real weld transverse section, for example nugget grain refinement or flow oscillations.

The trace of the weld seam is of particular interest as a potential weak point in a friction stir weld. According to Sato et al. [12], "A serious defect, associated with the oxide layer, is the "kissing-bond". The kissing-bond generally means a partial remnant of the unwelded butt surface.

There is another ring vortex effect: Intrusions of parent metal into otherwise fine grain nugget material, sometimes called "flow arms", are seen in transverse sections of friction stir welds near the weld shoulders as shown in Figure 5. Under hot welding conditions the "flow arms" are accentuated and a detrimental condition called "collapsed nugget" may result. Parent metal intrusions result when the radial inward velocity component v of the ring vortex flow counteracts the outward velocity component of the of the translational flow V, so that flow is into and not out of the rotating plug on the trailing surface ($\frac{x}{r} < 0$).

$$\frac{x}{r} < \frac{v}{V} \tag{9}$$

Since x is negative on the trailing surface, the only way inequality (9) can be satisfied is for negative values of v. Hence the intrusions occur next to the shoulder, where v is inward/negative, and not away from the shoulder, where v is outward/positive; this is as observed. Neglecting lateral shift [Equations (5) and (8)], the intrusions penetrate into the refined "nugget" metal from both sides to a depth

$$\Delta\left|\frac{y}{r}\right| = 1 - \sqrt{1 - \left(\frac{v}{V}\right)^2} \tag{10}$$

Note that the intrusion is zero if $v = 0$ and if $v = V$, all the way to the centerline, $\Delta\left|\frac{y}{r}\right| = 1$. If the lateral shift is taken into account, the intrusions are shifted toward the advancing side of the tool and the retreating side intrusion is exaggerated.

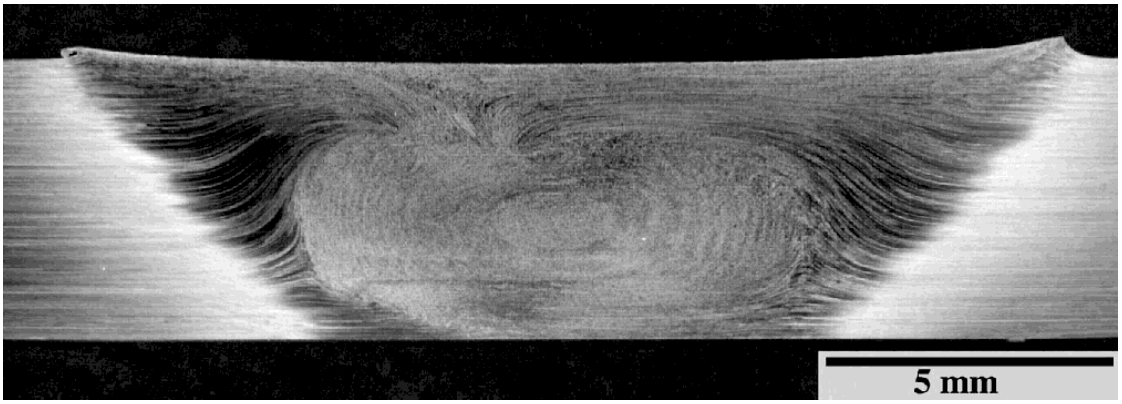

Figure 5. Flow arms (ring vortex/translational flow) at the top of a transverse section of conventional friction stir weld of in 5 mm thick 2195-T6 aluminum alloy courtesy of J. McClure, University of Texas at El Paso. A lateral shift toward the advancing side (ring vortex/rotating plug flow) on the left, axial displacements (ring vortex flow), and an "onion ring" band structure (oscillation) are visible.

Ring vortex effects are sensitive to tool design. Tools may be designed to produce multiple ring vortices or distorted ring vortices, with special structural effects. It is the ring vortex flow component that entrains contaminants on the weld metal surface and that may carry the contaminants deep into a weld. Ring vortex effects are also sensitive to RPM, through temperature and mechanical driving effects.

OSCILLATION EFFECTS

The kinetic FSW model presented a new opportunity for interpretation of various features exhibited by FS welds. Certain features implied an oscillation. One such

feature, periodic lateral displacements of the weld seam, has already been discussed and tentatively associated with oscillation of shear surface radius [Equations (4) and (5)]. Internal banding seen in transverse section as “onion rings” and surface striations in the wake of the tool called “tool marks” clearly associated with the banding in longitudinal section (See Figure 6) and in periodicity also implied an oscillation.

Although the presence of an oscillation has been established by strong circumstantial evidence for over a decade, an understanding of the mechanism responsible for the oscillation has only recently emerged [13]. F. Gratecap et al at the École Centrale de Nantes have proposed that the oscillation is caused by tool eccentricity.

Let us consider a sector bounded by planes passing through the axis of rotation of the pin and separated by angle $\Delta\theta$. The length and radius of the pin are w and R respectively. Suppose that a motion $\varepsilon \sin\omega t$ is imposed upon the pin, where ε is an eccentricity and ω is the angular velocity of the pin. Metal volume flow of $w\varepsilon \sin\omega t \Delta\theta$ is being pumped in and out of the sector. (We ignore phase differences for different sectors.) The metal is incompressible and the volume under the shoulder is fixed; hence it flows in and out periodically from under the shoulder edge so as to form the peaks and troughs of the “tool mark” striations. The shoulder moves with velocity V over a path width $R_S \Delta\theta \cos\theta$, where R_S is the shoulder radius and θ is the (fixed) angle of the sector. If the height of the striation is h, a balance of flow rates in and out of the sector requires:

$$h = \frac{w}{R_S} \frac{\varepsilon\omega}{V \cos\theta} \cos\omega t \qquad (11)$$

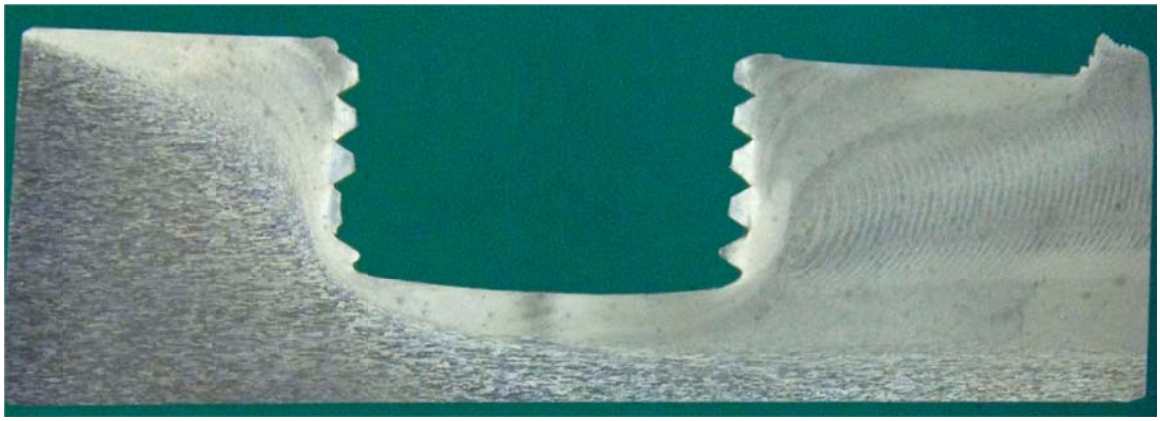

Figure 6. Formation of “tool marks” and internal banding. Lateral section of conventional friction stir weld cavity in 5 mm thick 2195-T6 aluminum alloy courtesy of J. McClure, University of Texas at El Paso. The lead angle of the tool is 3^o. “Tool marks” emerge from trailing edge of shoulder at right where the shear surface encounters the crown surface. Bands emerge from lower portion of shear surface where the ring vortex flow is outward. Bands do not emerge from the upper region of the trailing shear surface where the ring vortex flow is inward.

Presumably equation (9) breaks down at the weld edge where $\cos\theta \to 0$. To correct for the edge regions one would have to add to the $V\cos\theta$ term an estimate of an oozing rate out from under the shoulder perpendicular to the direction of motion. A cursory observation suggests that the striation heights vary with θ. Along the centerline where the tool displacement is $x = Vt$ and $\cos\theta = 1$, the contour (h vs. x) of the "tool marks" can be estimated:

$$h(\text{centerline}) = \frac{w}{R_S}\frac{\varepsilon\omega}{V}\cos\left(\frac{\omega}{V}x\right) \tag{12}$$

Further work needs to be done to understand banding and "tool marks". The contours of the "tool marks" don't seem to be sinusoidal. The banding contrast appears to be a result of deformation texture [14]. Presumably the textural distinctions are acquired as the pin pumps metal toward and away from the "tool mark" striations along the hottest and most easily deformed channels in the weld metal, i.e. along the shear surface. These channels are abandoned in the wake of the weld. In longitudinal section about a tool cavity they appear to be deformed by the ring vortex flow to bulge in the outflow region to form the "onion ring" band structure and to fall back into the shear surface and disappear in the inflow region close to the shoulder.

VARIETIES OF ROTATING PLUG

Conventional FSW rotating plugs start out as a blob on the bottom of a penetrating tool. Where the pressure P is low enough to permit it, slippage occurs, that is slippage occurs at:

$$P < \frac{\tau}{\mu} \tag{13}$$

where τ is the weld metal flow stress and μ is the coefficient of friction at the tool/weld metal interface. If the pressure is higher than inequality (13) permits, the surface seizes and shear in the weld metal takes over. Unlike the slip mechanism, the shear mechanism is not confined to the tool/weld metal interface, but can move out into the weld metal to reduce the torque required to rotate the tool and/or the penetration or translation force requirement. It may be anticipated that as a chain breaks at its weakest link Nature will select the shear surface shape easiest to deform, and the shapes of the shear surface may be estimated by minimal principles (i.e. calculus of variations).

As the pin penetrates deeper into the weld metal surface, metal must flow up to the surface to make room for it. At the surface the pressure is zero, but below the surface the pressure builds as it must force metal out against shearing resistance from the adjacent metal. Suppose that a smooth (not threaded) pin of radius r is being inserted into weld metal and that the pin slips at shear force μP. The metal upflow is taken to be in the shape of a hollow cylinder of thickness δ. The shear force on the external surface is taken to be τ. Along the slipping hollow cylinder the pressure P then changes with depth z according to:

$$\frac{dP}{dz} = \frac{\tau}{\delta}\left[\frac{\left(1+\frac{\delta}{r}\right)+\frac{\mu P}{\tau}}{1+\frac{1}{2}\frac{\delta}{r}}\right] \qquad (14)$$

The hollow cylinder flows up the tool between the uncapped weld crown surface and the immersed rotating plug. The hollow cylinder extruding past the penetrating pin is separated from the rotating plug by the shear surface just as the wake of the traveling pin is separated from its rotating plug. In both cases the separating shear surface is difficult to see as no significant volume structural change presents itself, as when parent metal suddenly becomes very fine-grained material upon passing through the shear surface. In the case of the hollow cylinder wake extending beyond the actual rotating plug at the bottom of the pin the shear surface separating the refined metal in the wake from the refined metal in the plug may be difficult to distinguish.

When the shoulder exerts sufficient pressure for the weld metal to stick to it as well as to the entire pin surface, the shear surface takes its familiar flared cylinder shape illustrated in Figure 7. At the edge of the shoulder, sticking tool contact gives way to slipping contact. The slipping area increases as the shoulder pressure is reduced. This reduces the flared region of the shear surface at the shoulder.

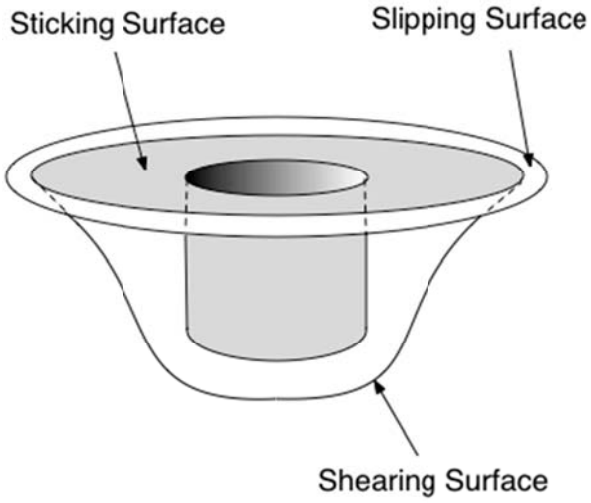

Figure 7. The rotating plug of weld metal sticks to the tool ($\mu P > \tau$) and shears past the stationary weld metal at the shear surface in the simplest FSW model. The part of the weld surface that slips ($\mu P < \tau$) is not part of the rotating plug. The sketch above represents the flared shear surface of an almost fully pressurized conventional FSW tool. As the axial plunge force on the tool is reduced, the sticking surface decreases and the slipping surface increases. At initial penetration with no shoulder contact, the sticking surface may be confined to the bottom of the pin. A relatively slow secondary flow throughout the rotating plug and neighboring weld metal volume may be taken into account in a more elaborate model.

J. Talia at Wichita State University introduced a fixed shoulder (detached from the pin) to enable high-rotational speed FSW by eliminating the excessive heating contribution of the rotating shoulder; a transverse weld structure [15] exhibiting a coarse structure around the pin and a refined nugget structure under the pin suggests slippage around the pin with attachment of a rotating plug to the bottom surface of the pin.

S. Guerdoux [16] has constructed a finite element model such that, “Figure 137 shows an example of a non-successful deposition in which case a void is formed at the lower advancing trailing side of the probe/matrix interface. It is to be noticed that the voids actually form on the advancing side in the actual process, for large range of alloys. Some voids may form periodically while other may result into so-called ‘worm holes’.” Radial symmetry of boundary conditions is disrupted.

THERMAL EFFECTS

If the slippage area on the tool is not large, the torque M required to rotate the tool is:

$$M = \int_{\substack{\text{Shear}\\ \text{Surface}}} 2\pi r^2 \tau \sqrt{dr^2 + dz^2} \tag{15}$$

The flow stress t is at the shear surface derives from a shear rate insensitive mechanism, otherwise, as for viscous constitutive equations, a shear surface discontinuity would be suppressed by shear rate variations. Metal flow stresses are in general not very strain rate dependent. The flow stress of a metal drops gradually from absolute zero temperature, falls precipitously at roughly half its melting temperature, and trails off to zero close to the melting temperature. Only the “trailing off” region is important for friction stir welding. Here the flow stress may be approximated roughly by a linear relation [17]:

$$\tau \sim \left(-\frac{\partial \tau}{\partial T}\right)\left(T_{melt} - T\right) \tag{16}$$

Suppose that the mechanical power supplied, $M\omega$, is dissipated as heat conducted away from the shear surface Q_{Cond} at temperature T and radius r into the weld metal at ambient temperature T_o and radius r_o through thermal conductivity k and also as heat required Q_{Conv} to bring metal of density r and specific heat C approaching the shear surface at weld speed V to the shear surface Temperature T. Let the tool pin radius be r, the length w, and the shoulder radius R_S.

$$\frac{2\pi R_S^3}{3}\left[1+\left(\frac{r}{R_S}\right)^2 \frac{w}{R_S}\right]\left(-\frac{\partial \tau}{\partial T}\right)\left(T_{melt} - T\right)\omega \sim \frac{2\pi k w}{\ln\frac{r_o}{r}}\left(T - T_o\right) + 2rw\rho C\left(T - T_o\right)V \tag{17}$$

Given values for all the tool dimensions and material properties, the weld parameters, and a rough estimate of r_o, to which the expression is not sensitive (it only appears in a logarithm), equation (17) allows an estimate of weld temperature.

Given a fixed temperature, it is possible to estimate the relationship between the weld speed and tool rotational speed for an isotherm:

$$V \sim -\left[\frac{\pi k}{r\rho C \ln\frac{r_o}{r}}\right] + \left\{\frac{\pi R_S^3}{3rw\rho C}\left[1+\left(\frac{r}{R_S}\right)^2\frac{w}{R_S}\right]\left(-\frac{\partial\tau}{\partial T}\right)\left(\frac{T_{melt}-T}{T-T_o}\right)\right\}\omega \qquad (18)$$

The (approximate) isotherms consist of a bundle of straight lines proceeding from a single point on the V-axis ($\omega = 0$). This is of particular interest because several years ago it was noticed that boundaries of the V-ω processing parameter window for sound welds also seemed to fall along straight lines proceeding from a single point on the V-axis and might be interpreted as isotherms. See Figure 8.

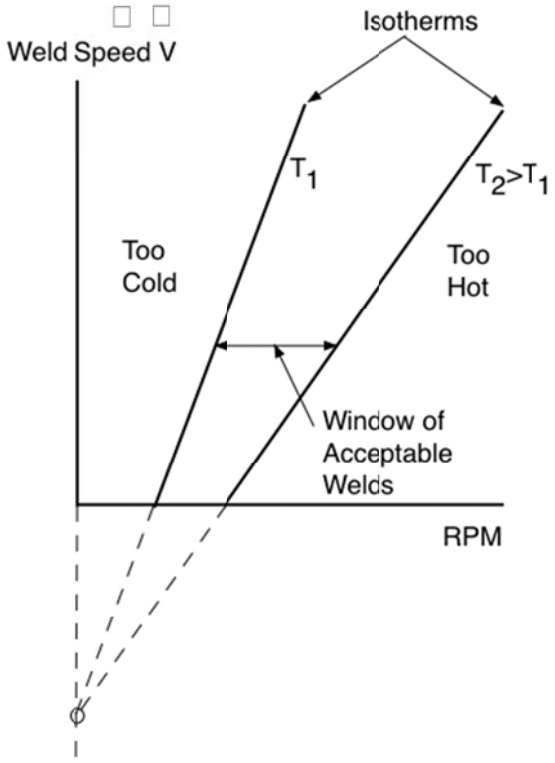

Figure 8. Approximate theoretical isotherms consist of a bundle of straight lines proceeding from a single point on the V-axis. This morphology roughly fits the boundaries of the processing parameter window.

Temperature limited parameter windows suggest flow-stress-based weld strength deterioration mechanisms. Flow stress is sensitive to temperature.

At low temperatures tool stresses are higher and could lead to breakage, but also the pressure required to force complete contact at the weld seam, approximately three times the tensile or six times the shear flow stress, rises with τ. If the pressure P at a point on the weld seam is significantly less than 6τ, cracks may be anticipated along the weld seam trace.

At high temperatures the flow stress is reduced. The soft metal may ooze out from under the shoulder as flash, reduce the internal pressure around the pin, and

create conditions for forming holes and trenches. Low melting phases may melt and be redistributed. With further study it may be possible to relate processing parameter boundaries to specific defects. A major focus of our current research is defect formation.

FORCES

Forces are a more difficult problem than torque. The drag force on a tool with minimal slippage area may be estimated by:

$$F_{Drag} \sim -\int_{\substack{\text{Shear}\\\text{Surface}}} \tau(\theta) r d\theta \sqrt{dr^2 + dz^2} \sin\theta + \int_{\substack{\text{Shear}\\\text{Surface}}} P(\theta) r d\theta dz \cos\theta \qquad (19)$$

But to compute the drag force one has to know how the shear stress τ and pressure P vary around the tool. Without such variation the drag of equation (19) is zero. More than one researcher has remarked to the author on how surprisingly low the FSW drag force can be. Rumors of negative drag (like an automobile wheel) exist, but the author is not aware of a well-attested case. One of the confusing things about drag force is that sometimes it drops with increasing tool RPM and sometimes it rises; over a broad range it may fall, then rise. This suggests two drag mechanisms operating together. Equation (19) has two parts, a shear drag and a pressure drag, which could be consonant with the observations. The drag force is not yet understood.

The lateral tool force is computed like the drag force, with similar difficulties. The plunge force of conventional FSW and the pinch force of self-reacting FSW require a knowledge of pressure variation with depth requiring computations like that of equation (14), but more elaborate.

Somewhat easier than absolute computations, estimates of perturbations in forces (or moments) due to an encounter with structures like holes, tack welds, thermal sinks (e.g. fixture hold-down clamps), etc. can be made through their effects on the shear surface.

CONCLUSIONS

In 1995 the solid-state FSW process was brought to MSFC with a view to overcoming fusion-welding difficulties of a new lithium-containing aluminum alloy mandated for the new Space Shuttle Lightweight External Tank. Study toward a comprehensive theoretical understanding of the friction stir process began at this time at MSFC. By 1999 the shear surface had been recognized and a kinematic model of the FSW process synthesized. From this time followed the semi-quantitative interpretation of a wide range of diverse FSW features, structural and thermo-mechanical.

It may be possible to increase the sharpness of the picture with Finite Element Modeling (FEM). Our studies suggest that: (1) the constitutive equation should include both a strain-rate insensitive and a strain-rate sensitive, temperature-dependent flow mechanism, and (2) the tool/workpiece boundary condition should be pressure-dependent, slipping above a pressure-dependent limiting shear stress and sticking below.

Whether or not resources permit the development of a more precise comprehensive FSW model, the existent semi-quantitative model with its illuminating images of process mechanisms and its implications for tool design and parameter selection is available at MSFC as a conceptual tool for FSW process engineering as-is or with further development.

REFERENCES

1. A.C. Nunes, Jr. “Welding As Science: Applying Basic Engineering Principles to the Discipline.” *NASA Technical Memorandum: NASA/TM-2010-216449*, 2010.

2. A.P. Reynolds, T.U. Seidel, and M. Simonsen. “Visualization of Material Flow in an Autogenous Friction Stir Weld.” *1st International Symposium on Friction Stir Welding*, Rockwell Science Center, Thousand Oaks, CA. June 14-16, 1999.

3. K. Colligan. “Material Flow Behavior during Friction Stir Welding of Aluminum.” *Welding Journal* 78(7) 229-s to 237-s. 1999.

4. P.L.B. Oxley. *The Mechanics of Machining: An Analytical Approach to Assessing Machinability.* John Wiley & Sons (first published by Ellis Horwood Limited) 23-36, 1989.

5. Travis L. Brown, Srinivasan Swaminathan, Srinivasan Chandrasekar, W. Dale Compton, Alexander H. King, and Kevin P.Trumble. “Low-cost manufacturing process for nanostructured metals and alloys.” *Journal of Materials Research* 17(10) 2484-2482, 2002.

6. T.W. Wright, *The Physics and Mathematics of Adiabatic Shear Bands*. Cambridge University Press, 2002.

7. A.C. Nunes, Jr. “Prolegomena to the Study of Friction Stir Welding.” *Materials Science & Technology 2010*. Houston, TX. October 17-21, 2010.

8. A.C. Nunes, Jr., E.L. Bernstein, and J.C. McClure. “A Rotating Plug Model for Friction Stir Welding.” *81st AWS Annual Convention*, Chicago, IL, April 25-28, 2000.

9. Arthur C. Nunes, Jr. “Friction Stir Welding at MSFC: Kinematics.” *4th Conference on Aerospace Materials, Processes, and Environmental Technology*, Huntsville, AL. September 18-20, 2000

10. Arthur C. Nunes, Jr. “Flow in the Proximity of the Pin-Tool in Friction Stir Welding and Its Relation to Weld Homogeneity.” *37th Annual Technical Meeting of the Society of Engineering Science*, University of South Carolina, Columbia, SC, October 23-25, 2000.

11. Arthur C. Nunes, Jr. “Wiping Metal Transfer in Friction Stir Welding.” *Aluminum 2001: Proceedings of the 2001 TMS Annual Meeting Automotive Alloys and Joining Aluminum Symposia.* (New Orleans, LA, February 11-15). Edited by G. Kaufmann, J Green, and S. Das. TMS (The Minerals, Metals & Materials Society), 235-248, 2001.

12. Yutaka S. Sato, Hideki Takauchi, Seung C. Park, Hiroyuki Kokawa. “Characteristics of the kissing-bond in friction stir welded Al alloy 1050.” *Materials Science and Engineering* A 405, 333-338, 2005.

13. F. Gratecap, M. Girard, S. Marya, and G. Racineux. “Exploring material flow in

friction stir welding: Tool eccentricity and formation of banded structures." (Published online: 11 January 2011) *International Journal of Material Forming*, DOI 10.1007/s12289-010-1008-5 © Springer-Verlag France 2011.

14. J.A. Schneider and A.C.Nunes, Jr. "Characterization of plastic flow and resulting microtextures in a friction stir weld." *Metallurgical and Materials Transactions B*. 35B(4), 777-783, 2004.

15. C.A. Widener, J.E. Talia, B.M. Tweedy, and D.A. Buford. "High-Rotational Speed Friction Stir Welding with a Fixed Shoulder." Paper 38, *6th International Symposium on Friction Stir Welding, Saint-Sauveur*, Nr Montreal, Canada, October 10-13, 2006.

16. S. Guerdoux. "Numerical Simulation of the Friction Stir Welding Process." *Doctoral Thesis. École des Mines de Paris. Spécialité "Mécanique Numérique"*. 13 December 2007.

17. A.R.E. Singer and S.A. Cottrell. "Properties of Aluminum-Silicon Alloys at Temperatures in the Region of the Solidus." *Journal of the Institute of Metals* 73, 33-73, 1947.

LIST OF SYMBOLS

C	specific heat of weld metal
F_{Drag}	drag force on pin or tool
h	height of metal discharge from under tool shoulder
k	thermal conductivity of weld metal
M	moment or torque on tool
P	pressure
Q_{Cond}	heat conducted away from tool into environment
Q_{Conv}	heat convected away from tool
r	radial coordinate from center of shear surface
r_o	radial coordinate from center of shear surface to approximately ambient temperature
R_S	radius of tool shoulder
T	temperature
T_{melt}	melting temperature of weld metal
T_o	ambient temperature
v	radial velocity component
V	weld speed
$\vec{V}$	vector velocity field
w	length of friction stir pin
x	coordinate from center of shear surface in direction of weld motion
y	coordinate from center of shear surface toward retreating side of tool
z	axial coordinate along pin
$\dot{\gamma}$	rate of shear
ε	eccentricity of tool

δ 1. thickness across shear surface [Equation (1)]; 2. thickness of eccentric portion of rotating plug [Equation (6)]; 3. thickness of metal upflow region around tool [Equation (14)]

μ coefficient of friction

θ angular coordinate from direction of weld motion

ρ density of weld metal

τ shearing flow stress

ω angular velocity of rotating plug

$\left(-\frac{\partial\tau}{\partial T}\right)$ drop in shear flow stress per unit rise in temperature close to melting temperature (taken as an approximate constant)

FIGURE CAPTIONS

1. Midsectional plan-view of macrostructure around FSW pin, tool spindle rotating counterclockwise at 220 RPM, travel to the right at 3.5 inches per minute in 0.317 inches thick 2219-T87 aluminum alloy. The weld was suddenly stopped and the pin backed out of its cavity, which has been replaced by a bubble-filled mounting medium. Note the very sudden refinement in structure at the shear surface. Note the increased thickness of the rotating plug of weld metal beneath the shear surface on the retreating edge of the pin to accommodate backflow of metal around the pin. In sections closer to the shoulder the shear surface moves out to enclose a wider expanse of rotating plug metal.

2. Early presentation (internal 14 February 2000) of the rotating plug model. A segment of the line of marching figures marches across a merry-go-round platform and is whisked forward. A similar displacement occurs when a rotating plug runs through a tracer line [2].

3. Lateral weld seam oscillation on plan-view of bimetallic FS weld: 2219 aluminum alloy on upper (advancing) side, 2195 on lower (retreating) side courtesy of G. Bjorkman of Lockheed Martin. Pin site (central hole) is 12.7 mm (0.5 inch) in diameter. The straight, unwelded seam on the right of the central hole becomes the wavy, welded seam on the left. While the 2219 metal appears to have entered the shear surface and been subjected to the grain refinement produced by its high shear rate, the 2195 metal appears to have been rotated around the tool in a slower peripheral flow resulting in a broader flow region and retaining more of the parent metal structural features.

4. Schematic “tongue and groove” structure of bimetallic self-reacting weld. Where the ring vortex flow is radially inward the seam trace is held longer in the rotating plug and consequently is shifted toward the advancing side of the weld. At the weld center the ring vortex flow is radially outward, the seam trace is jettisoned sooner to the wake, and the seam trace is shifted to the retreating side of the weld. This sketch shows only general trends and not the usual complications that round off and distort the seam trace. Nor does it show other features that would be superimposed upon a real weld transverse section, for example nugget grain refinement or flow oscillations.

5. Flow arms (ring vortex/translational flow) at the top of a transverse section of conventional friction stir weld of in 5 mm thick 2195-T6 aluminum alloy courtesy of J.

McClure, University of Texas at El Paso. A lateral shift toward the advancing side (ring vortex/rotating plug flow) on the left, axial displacements (ring vortex flow), and an “onion ring” band structure (oscillation) are visible.

6. Formation of “tool marks” and internal banding. Lateral section of conventional friction stir weld cavity in 5 mm thick 2195-T6 aluminum alloy courtesy of J. McClure, University of Texas at El Paso. The lead angle of the tool is 3^{o}. “Tool marks” emerge from trailing edge of shoulder at right where the shear surface encounters the crown surface. Bands emerge from lower portion of shear surface where the ring vortex flow is outward. Bands do not emerge from the upper region of the trailing shear surface where the ring vortex flow is inward.

7. The rotating plug of weld metal sticks to the tool ($\mu P > \tau$) and shears past the stationary weld metal at the shear surface in the simplest FSW model. The part of the weld surface that slips ($\mu P < \tau$) is not part of the rotating plug. The sketch above represents the flared shear surface of an almost fully pressurized conventional FSW tool. As the axial plunge force on the tool is reduced, the sticking surface decreases and the slipping surface increases. At initial penetration with no shoulder contact, the sticking surface may be confined to the bottom of the pin. A relatively slow secondary flow throughout the rotating plug and neighboring weld metal volume may be taken into account in a more elaborate model.

8. Approximate theoretical isotherms consist of a bundle of straight lines proceeding from a single point on the V-axis. This morphology roughly fits the boundaries of the processing parameter window.

The Evolution of Friction Stir Welding Theory at Marshall Space Flight Center

Arthur C. Nunes, Jr.
Materials and Processes Laboratory
Marshall Space Flight Center,
Huntsville, AL

Acknowledgements

The sequence of concepts presented here ultimately rests upon people. Over the years we have accumulated debts for data, discussions, and helpfulness to:

A.P. Reynolds of the University of South Carolina

G.E. Cook of Vanderbilt University

J.C. McClure of the University of Texas at El Paso

The Late J. Talia of Wichita State University

Q.H. Zuo of the University of Alabama in Huntsville

J.A. Schneider of Mississippi State University

We are heavily indebted to NASA's Summer Faculty Research Program, the Graduate Student Research Program (the latest doctoral students being Tracie Prater of Vanderbilt and Haley Doude of MSU), and the Student Internship Program.

Although the above debts come to immediate consciousness, they rest upon a mountain of debt deserving recognition, but unrecognized here.

A Note on Method

1. Visualize a basic conceptual model. Start as simply as possible.

2. Construct a mathematical representation of the model. Note:

    a) Parametric trend effects.

    b) Computed numerical magnitudes.

3. Critique the model. Look for modifications leading to greater verisimilitude.

4. Visualize a new model and repeat.

Summary

1995 FSW studies begin at MSFC

1999 Annus Mirabilis:

- Discovery of
  - Shear Surface and Rotating Plug
  - Wiping Metal Transfer
  - Ring Vortex Circulation
- Synthesis of
  - Kinematic FSW Flow Model

2000 Applications begin with Explanations of Tracer Patterns

2004 Oscillation Effects and FSW Band Structure

2010 Extension to Thermal and Dynamic Analyses:

- Discovery of
  - Isotherm Parameter Window Boundaries

Shear Surface and Rotating Plug

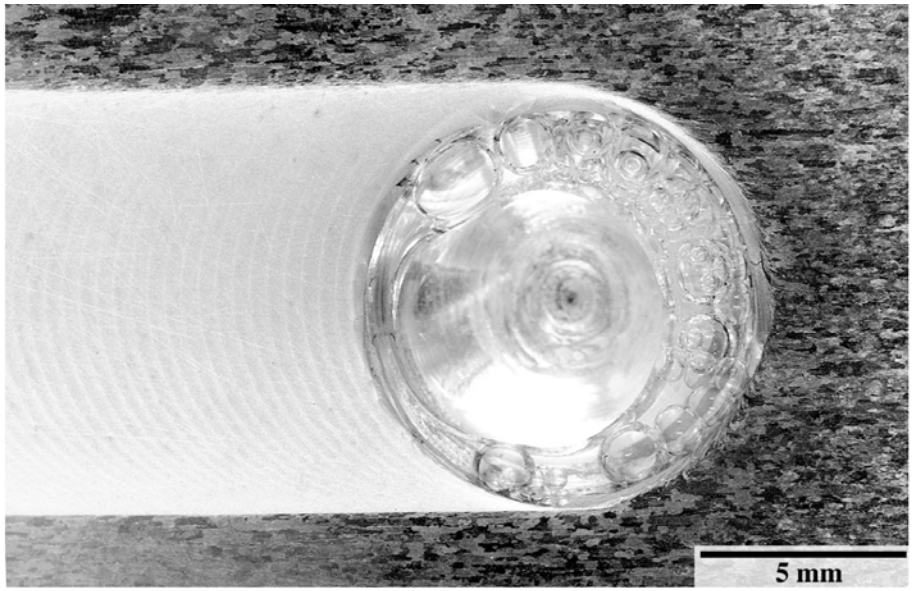

Figure 1. Midsectional plan-view of macrostructure around FSW pin, tool spindle rotating counterclockwise at 220 RPM, travel to the right at 3.5 inches per minute in 0.317 inches thick 2219-T87 aluminum alloy. The weld was suddenly stopped and the pin backed out of its cavity, which has been replaced by a bubble-filled mounting medium. Note the very sudden refinement in structure at the shear surface. Note the increased thickness of the rotating plug of weld metal beneath the shear surface on the retreating edge of the pin to accommodate backflow of metal around the pin. In sections closer to the shoulder the shear surface moves out to enclose a wider expanse of rotating plug metal.

Shear Surface and Rotating Plug

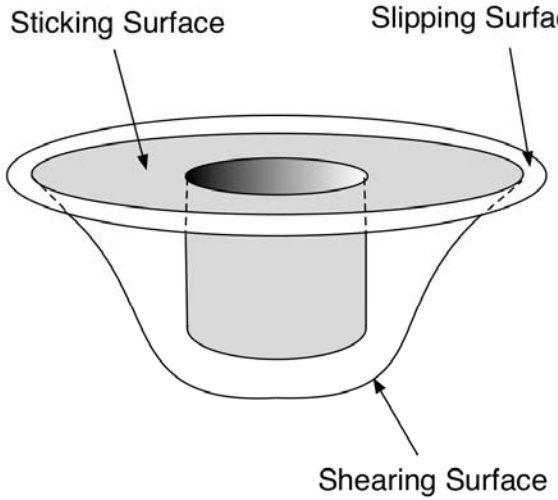

Figure 7. The rotating plug of weld metal sticks to the tool ($\mu P > \tau$) and shears past the stationary weld metal at the shear surface in the simplest FSW model. The part of the weld surface that slips ($\mu P < \tau$) is not part of the rotating plug. The sketch above represents the flared shear surface of an almost fully pressurized conventional FSW tool. As the axial plunge force on the tool is reduced, the sticking surface decreases and the slipping surface increases. At initial penetration with no shoulder contact, the sticking surface may be confined to the bottom of the pin. A relatively slow secondary flow throughout the rotating plug and neighboring weld metal volume may be taken into account in a more elaborate model.

Streamlines & Shear Surface Mathematical Representation

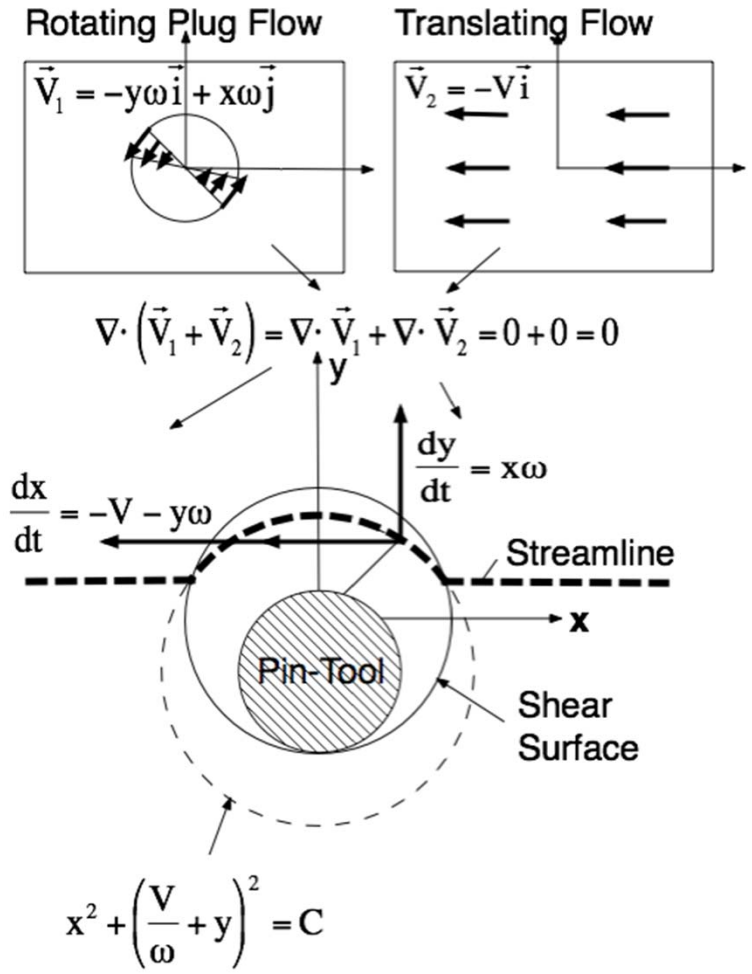

Rotating Plug Displacements

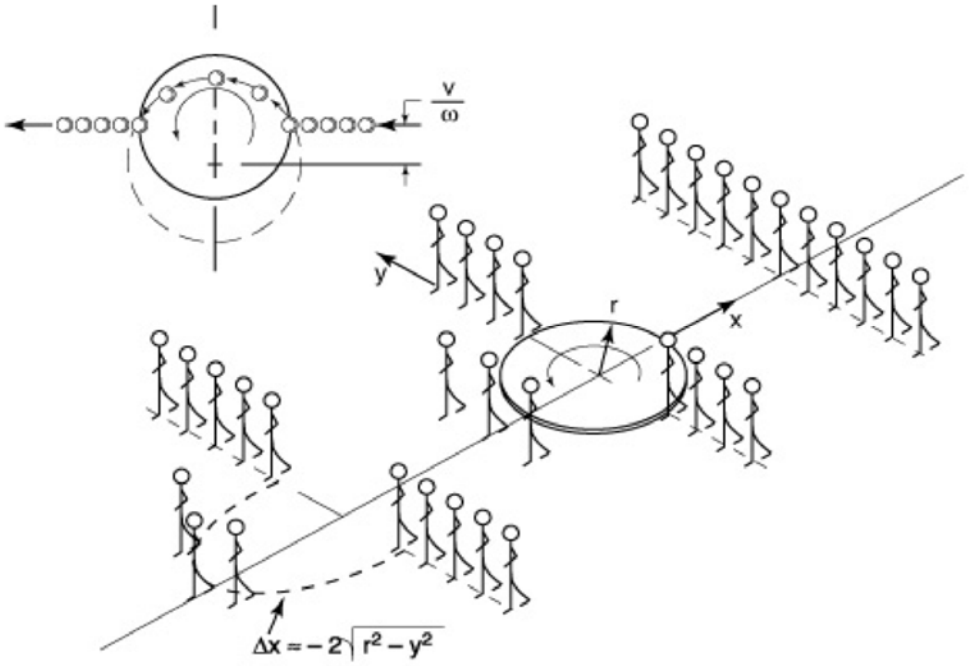

Figure 2. Early presentation (internal 14 February 2000) of the rotating plug model. A segment of the line of marching figures marches across a merry-go-round platform and is whisked forward. A similar displacement occurs when a rotating plug runs through a tracer line [2].

Ring Vortex Displacements of Weld Seam

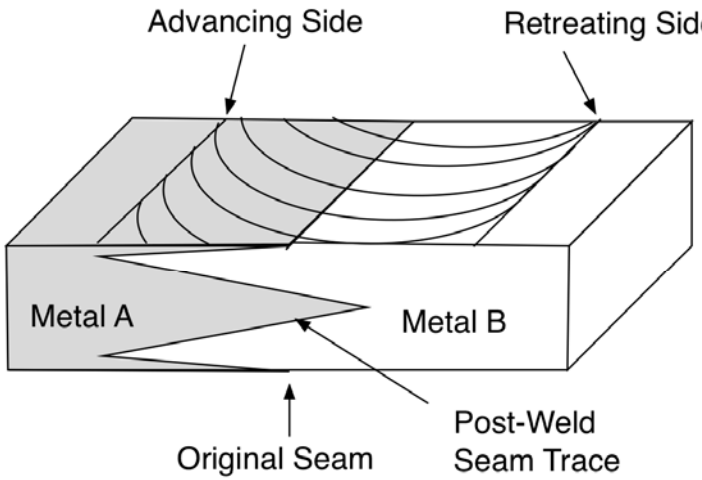

$$\frac{y}{r} \sim \frac{y_o}{r_o} + \frac{v}{V}(\theta - \theta_o)$$

Figure 4. Schematic "tongue and groove" structure of bimetallic self-reacting weld. Where the ring vortex flow is radially inward the seam trace is held longer in the rotating plug and consequently is shifted toward the advancing side of the weld. At the weld center the ring vortex flow is radially outward, the seam trace is jettisoned sooner to the wake, and the seam trace is shifted to the retreating side of the weld. This sketch shows only general trends and not the usual complications that round off and distort the seam trace. Nor does it show other features that would be superimposed upon a real weld transverse section, for example nugget grain refinement or flow oscillations.

Shear Surface Oscillation Effect

$$\frac{y}{r} \sim \frac{y_o}{r_o} - \frac{\omega \Delta r}{V} \sin(\theta - \theta_o)$$

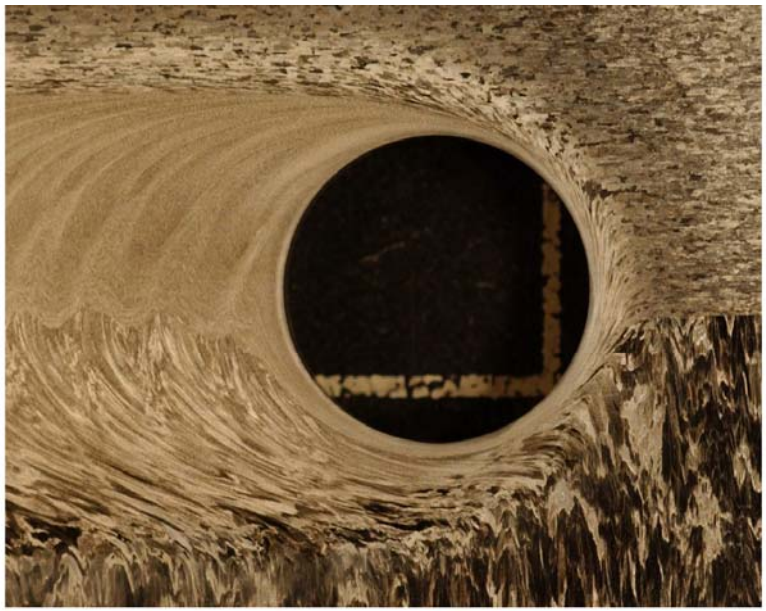

Figure 3. Lateral weld seam oscillation on plan-view of bimetallic FS weld: 2219 aluminum alloy on upper (advancing) side, 2195 on lower (retreating) side courtesy of G. Bjorkman of Lockheed Martin. Pin site (central hole) is 12.7 mm (0.5 inch) in diameter. The straight, unwelded seam on the right of the central hole becomes the wavy, welded seam on the left. While the 2219 metal appears to have entered the shear surface and been subjected to the grain refinement produced by its high shear rate, the 2195 metal appears to have been rotated around the tool in a slower peripheral flow resulting in a broader flow region and retaining more of the parent metal structural features.

Oscillation Banding and "Tool Marks" with Ring Vortex Distortion

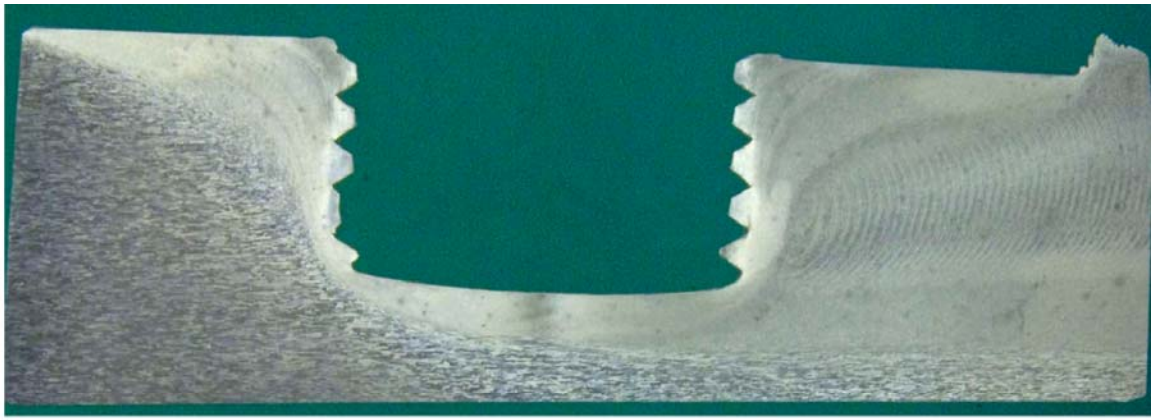

Figure 5. Formation of "tool marks" and internal banding. Lateral section of conventional friction stir weld cavity in 5 mm thick 2195-T6 aluminum alloy courtesy of J. McClure, University of Texas at El Paso. The lead angle of the tool is 3^{o}. "Tool marks" emerge from trailing edge of shoulder at right where the shear surface encounters the crown surface. Bands emerge from lower portion of shear surface where the ring vortex flow is outward. Bands do not emerge from the upper region of the trailing shear surface where the ring vortex flow is inward.

Ring Vortex Flow Arms and Lateral Displacement

$$\Delta\left|\frac{y}{r}\right| = 1 - \sqrt{1 - \left(\frac{v}{V}\right)^2}$$

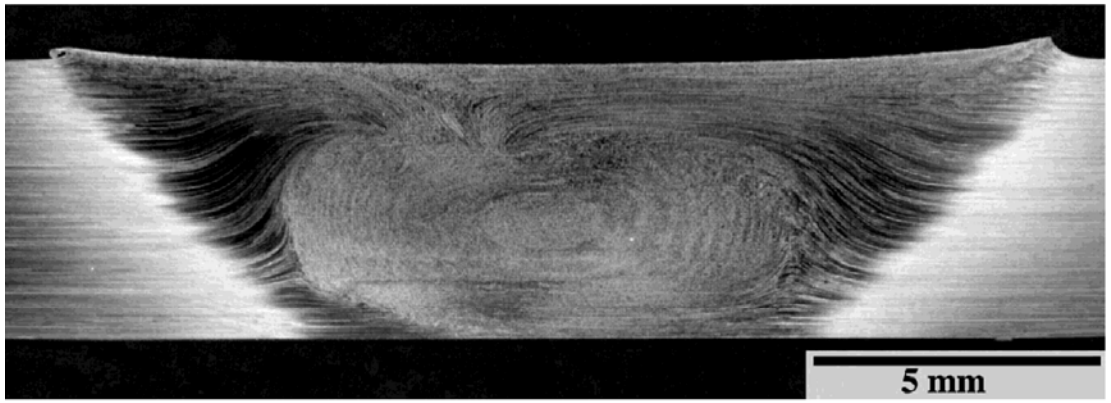

Figure 5. Flow arms (ring vortex/translational flow) at the top of a transverse section of conventional friction stir weld of in 5 mm thick 2195-T6 aluminum alloy courtesy of J. McClure, University of Texas at El Paso. A lateral shift toward the advancing side (ring vortex/rotating plug flow) on the left, axial displacements (ring vortex flow), and an "onion ring" band structure (oscillation) are visible.

Dynamic Application: Drag Force

$$F_{Drag} \sim -\int_{\substack{\text{Shear}\\\text{Surface}}} \tau(\theta) r d\theta \sqrt{dr^2 + dz^2} \sin\theta + \int_{\substack{\text{Shear}\\\text{Surface}}} P(\theta) r d\theta dz \cos\theta$$

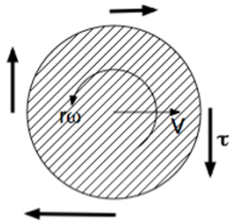

SHEAR DRAG

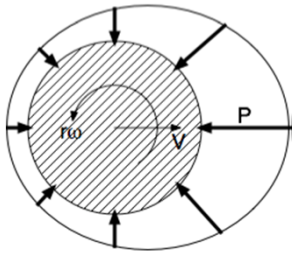

PRESSURE DRAG

Dynamic Application: Temperature

$$V \sim -\left[\frac{\pi k}{r\rho C \ln\frac{r_o}{r}}\right] + \left\{\frac{\pi R_S^3}{3rw\rho C}\left[1+\left(\frac{r}{R_S}\right)^2\frac{w}{R_S}\right]\left(-\frac{\partial\tau}{\partial T}\right)\left(\frac{T_{melt}-T}{T-T_o}\right)\right\}\omega$$

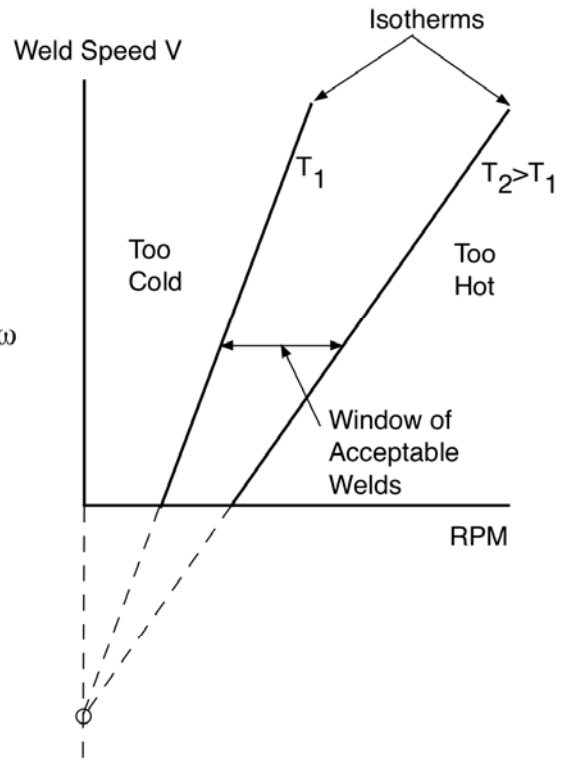

Figure 8. Approximate theoretical isotherms consist of a bundle of straight lines proceeding from a single point on the V-axis. This morphology roughly fits the boundaries of the processing parameter window.

Conclusions

By 1999 the shear surface had been recognized and a kinematic model of the FSW process synthesized. This was followed by the semi-quantitative interpretation of a wide range of diverse FSW features, structural and thermo-mechanical.

Finite Element Modeling (FEM) may increase the sharpness of the picture. An FEM model should incorporate:

1. A dual (plastic and viscous flow) constitutive equation,
2. Pressure sensitive stick-or-slip boundary conditions.

The imagery inherent in the existent MSFC model makes it a potentially especially useful conceptual tool for FSW tool design, parameter selection, and interpretation of weld structural features.